Multifunctional characteristics of 3D printed polymer nanocomposites under monotonic and cyclic compression

Pawan Verma, Jabir Ubaid, Fahad Alam, Suleyman Deveci, S. Kumar

PII: S2214-9147(23)00140-X

DOI: https://doi.org/10.1016/j.dt.2023.05.017

Reference: DT 1257

To appear in: *Defence Technology*

Received Date: 16 July 2022

Revised Date: 11 May 2023

Accepted Date: 26 May 2023

Please cite this article as: Verma P, Ubaid J, Alam F, Deveci S, Kumar S, Multifunctional characteristics of 3D printed polymer nanocomposites under monotonic and cyclic compression, *Defence Technology* (2023), doi: https://doi.org/10.1016/j.dt.2023.05.017.

Multifunctional characteristics of 3D printed polymer nanocomposites under monotonic and cyclic compression

Pawan Verma [a], Jabir Ubaid [a], Fahad Alam [a], Suleyman Deveci [b], S Kumar [c,*]

[a] Department of Mechanical Engineering, Khalifa University of Science and Technology, Masdar Institute, Masdar City, P.O. Box 54224, Abu Dhabi, United Arab Emirates

[b] Borouge Pte. Ltd., Innovation Centre, Sas Al Nakhl, 6951 Abu Dhabi, United Arab Emirates

[c] James Watt School of Engineering, University of Glasgow, Glasgow, G12 8QQ, UK

***Corresponding author:** S Kumar

E-mail: msv.kumar@glasgow.ac.uk; s.kumar@eng.oxon.org

Multifunctional characteristics of 3D printed polymer nanocomposites under monotonic and cyclic compression

Pawan Verma[1], Jabir Ubaid[1], Fahad Alam[1], Suleyman Deveci[2], S Kumar[3]*

[1]Department of Mechanical Engineering, Khalifa University of Science and Technology, Masdar Institute, Masdar City, P.O. Box 54224, Abu Dhabi, United Arab Emirates

[2]Borouge Pte. Ltd., Innovation Centre, Sas Al Nakhl, 6951 Abu Dhabi, United Arab Emirates

[3]James Watt School of Engineering, University of Glasgow, Glasgow, G12 8QQ, UK

Abstract

This study presents the multifunctional characteristics of multi-walled carbon nanotube (MWCNT)/polypropylene random copolymer (PPR) composites enabled via fused filament fabrication (FFF) under monotonic and quasi-static cyclic compression. Utilizing in-house MWCNT-engineered PPR filament feedstocks, both bulk and cellular composites were realized. The morphological features of nanocomposites were examined via scanning electron microscopy, which reveals that MWCNTs are uniformly dispersed. The uniformly dispersed MWCNTs forms an electrically conductive network within the PPR matrix, and the resulting nanocomposite shows good electrical conductivity (~10^{-1}S/cm), improved mechanical performance (modulus increases by 125% and compressive strength increases by 25% for 8 wt.% MWCNT loading) and pronounced piezoresistive response (gauge factor of 27.9-8.5 for bulk samples) under compression. The influence of strain rate on the piezoresistive response of bulk samples (4 wt.% of MWCNT) under compression was also measured. Under repeated cyclic compression (2% constant strain amplitude), the nanocomposite exhibited stable piezoresistive performance up to 100 cycles. The piezoresistive response under repeated cyclic loading with increasing strain amplitude of was also assessed. The gauge factor of BCC and FCC cellular composites (4 wt.%

of MWCNT) with a relative density of 30% was observed to be 46.4 and 30.2 respectively, under compression. The higher sensitivity of the BCC plate-lattice could be attributed to its higher degree of stretching-dominated deformation behavior than the FCC plate-lattice, which exhibits bending-dominated behavior. The 3D printed cellular PPR/MWCNT composites structures were found to show excellent piezoresistive self-sensing characteristics and open new avenues for *in situ* structural health monitoring in various applications.

Keywords: carbon nanotubes, nanoengineered polymer composites, 3D printing, piezoresistive self-sensing, lattice structures

1. Introduction

Carbon nanotube (CNT)-based polymer composites are very promising materials for numerous functional applications compared to other carbonous fillers as CNTs can form conductive networks/paths within the insulating matrix at very low loading. The percolated conductive paths are responsible for the electron movement within the insulating matrix [1, 2]. This ability has been utilized for designing smart materials which can sense *in situ* strain and/or damage state through change in resistance of the material under stress or strain [3-6]. Conducting networks within the polymer matrix behave like an artificial nervous system (ANS) to detect strain changes in a structure at distribution points [7]. A CNT based ANS may therefore useful for applications such as structural health monitoring, smart building, skin-mountable and wearable electronic devices and robotics [7].

In addition, the performance of ANS can be tailored by changing the matrix material, architectural design, and CNT loading. However, the main challenge is to enable ANS and fabrication of complex structures with ANS morphology. In this context, additive manufacturing (AM), also known as 3D printing, is considered as a promising and innovative technology for

fabricating complex structures that are difficult and/or impossible to produce via conventional methods [8, 9] [10]. Over the years, several AM techniques such as inkjet printing, powder bed fusion, contour crafting [11], fused filament fabrication (FFF) [12, 13] etc., have been developed. Among all extant 3D printing techniques, FFF is getting more recognition due to its operational simplicity and low cost [10, 14-18]. The feedstock used in the FFF process is in the form of a continuous filament of thermoplastic polymer. Commonly used polymers and their composites for FFF process are polylactic acid (PLA)[19], acrylonitrile butadiene (ABS)[20, 21], polyamide (PA)[22], polycarbonate (PC)[23], and polystyrene (PS)[24] etc. As the demand for polymer composites with functional properties is increasing day by day, the need for developing printable materials with functional properties is also constantly increasing.

As evidenced by the growing number of studies, AM is becoming a viable method for creating materials/structures with desirable mechanical and functional properties. Several studies focused on the creation of bulk composite materials using a variety of materials, including soft and stretchable composite materials such as PDMS/MWCNT[25] and TPU/CNT[26] and stiffer composite materials like PP/CNT[27] and PEEK/CNT[13] and investigated their mechanical and piezoresistive performance. Additionally, these studies have also successfully created periodic cellular composites by utilizing the capability of AM to create complex geometries in a single production process[13, 27]. These studies on cellular composites demonstrated self-sensing functionalities in addition to enhanced mechanical attributes.

This study explores the multifunctional properties of highly loaded polypropylene random copolymers (PPR)/multi-walled carbon nanotube (MWCNT) composites (up to 8 wt%). The PPR/MWCNT filaments were developed by melt-blending using a twin-screw extruder. Both bulk and cellular structures were successfully fabricated using FFF and their piezoresistive self-sensing

characteristics were measured under quasi-static monotonic and cyclic compression. The effects of MWCNTs on electrical conductivity and mechanical properties were systematically investigated. The state of dispersion of MWCNTs in the PPR matrix was investigated by scanning electron microscopy, while AC electrical conductivity and compressive piezoresistive performance were studied to investigate the strain and damage sensing behavior of the bulk and cellular composites. In addition, cyclic loading/unloading tests under constant strain amplitude and increasing strain amplitude were performed to evaluate the long-term self-sensing performance of the composites. Cellular structures with two different closed-cell architectures, namely BCC plate-lattice and FCC plate-lattice, were fabricated to investigate the effects of the cellular architectures on the mechanical and self-sensing performance of the composites.

2. Materials and experimental methods

2.1 Materials

Polypropylene-co-ethylene random copolymer (PPR) (melt flow index of 0.3g/10 min at 230 ^{o}C/2.16 kg) supplied by Borouge Pte. Ltd., was used as the matrix. The PPR was used instead of PP (homopolymer) for the present study because it is comparatively inexpensive and has low processing (low melting temperature ~147 °C) temperature and comparable mechanical properties to that of PP [27, 28]. The MWCNTs supplied by Applied Nanostructured Solution, LLC were used as conductive fillers. The MWCNTs were grown on glass fiber substrates by chemical vapor deposition (CVD) [28]. The average outer diameter and length of the MWCNTs were ~12 nm and ~30 µm, respectively [29]. Thermogravimetric analysis (TGA) was used to determine the purity of the MWCNTs and was found to be 86%

2.2 Preparation of PPR/MWCNT composite filaments for FFF 3D printing

The PPR/MWCNT composite filaments were prepared using a co-rotating twin screw extruder (Coperion ZSK 18, Germany) (see Fig.1) with a screw length to screw diameter (L/D) ratio of 40. The processing parameters selected for the fabrication of feedstock filaments are summarized in Table S1. Prior to processing, PPR and MWCNTs were vacuum dried at 80 °C for 6 hours. The polymer composites were extruded through a circular die of 1.80 mm. A roller was used to maintain the consistency of the filament diameter (i.e., 1.75 mm). The PPR/MWCNT composites were prepared by mixing 0, 4, 6, 8 wt.% of MWCNT and are identified as PPR-0, PPR-4, PPR-6, and PPR-8, respectively.

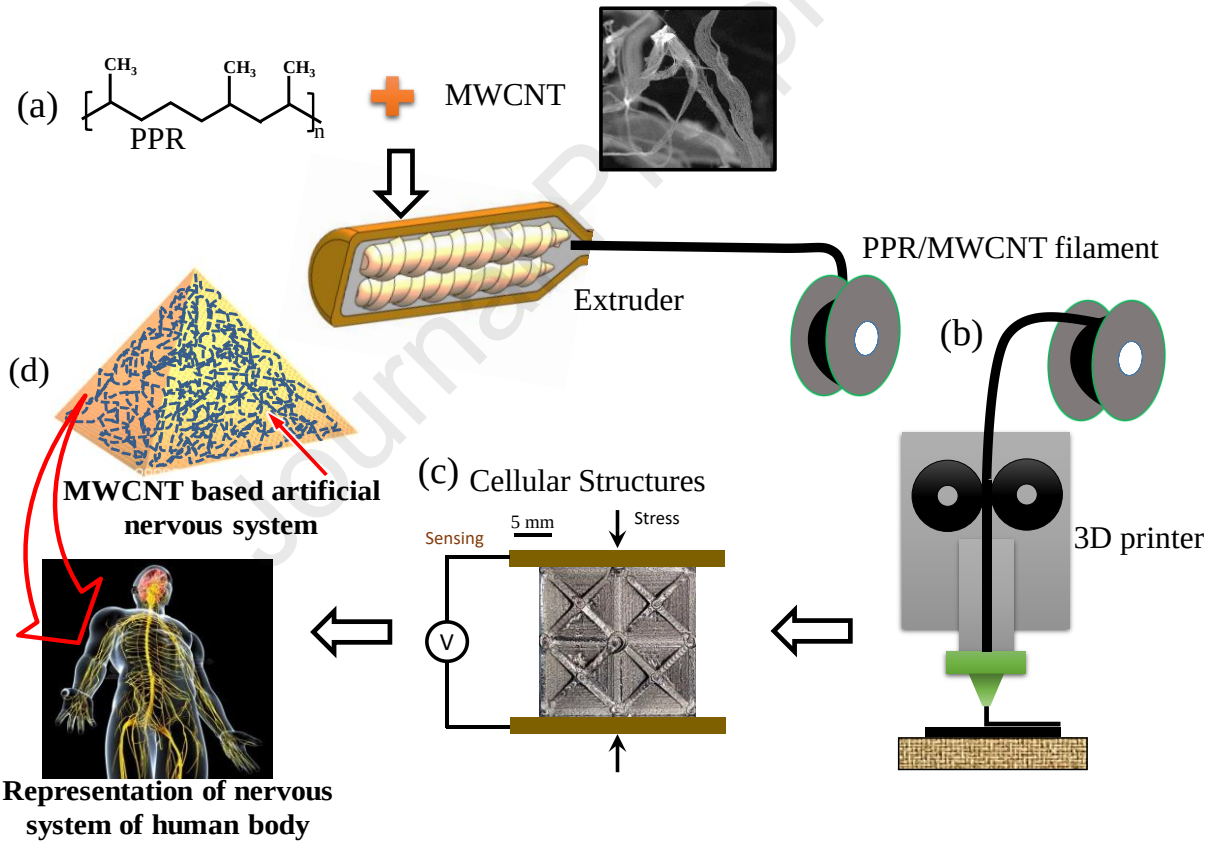

Fig.1 Schematic diagram of filament fabrication and 3D printing :(a) extruder, (b) FFF 3D printer, (c) 3D printed cellular structures and (d) MWCNT based artificial nervous system (ANS)

2.3. Fabrication of dense and cellular nanocomposites via FFF 3D printing

Creator Pro FFF 3D printer (Zhejiang Flashforge 3D technology Co., LTD, Zhejiang, China) with a nozzle diameter of 0.4 mm was used to make the test samples using in-house made filaments. CAD models were created using Solidworks (Dassault Systèmes Corp.) and converted to 3D printable STL files. The process parameters for fabricating the test samples are listed in Table S2. For the fabrication of PPR /MWCNT composites, the 3D printer bed was replaced with a metallic bed and a pressure sensitive PP (Polypropylene) tape was used to overcome the warpage problem associated with its poor adhesion to print bed.

2.4. Characterization and testing of dense and cellular nanocomposites

Scanning electron microscopy (Nova Nano SEM 50 series) was used to investigate the dispersion state of MWCNTs in the PPR matrix using cryogenically fractured samples. Prior to characterization, the samples were coated with a thin layer of gold. The electrical conductivity of the composites was measured using a GW Instek LCR meter. The samples with a size of 23×11×2 mm^3 were tested using an Agilent E16451B probe at a frequency of 1000 Hz. The compressive mechanical tests were performed on cuboidal (25×12.5×12.5 mm^3) specimens and BCC and FCC cellular structures using a Zwick-Roell universal testing machine. Real-time piezoresistive tests were performed using a universal testing machine (Zwick-Roell) with an electrometer (Tektronix DMM 4050). Piezoresistive performance under uniaxial compression was measured at different strain rates, i.e., 5, 15, and 25 mm/min. Similarly, the piezoresistive response under repeated cyclic loading with a constant strain amplitude of 2% at a crosshead speed of 5 mm/min was investigated. The piezoresistive responses under cyclic loading with increased strain amplitude were also studied at a crosshead speed of 5 mm/min. For this analysis, the strain amplitude was kept at 2% for the first cycle and increased by 1% for each successive cycle. Cellular structures with two different closed-cell architectures, namely BCC plate-lattices and FCC plate-lattices were

additively manufactured using PPR-4 and the effect of unit cell topology on out-of-plane mechanical and self-sensing performance of the cellular structure under quasi-static compression is evaluated. The fabricated specimens consist of 2×2×2 unit cells with a cell size of 10 mm and a relative density of 30%.

3. Results and discussion

3.1 Morphological characterization using scanning electron microscopy (SEM)

Fig. 2a-c shows SEM scans of PPR/MWCNT composites with varying MWCNT loading, while the inset images show SEM scans of the same composition at higher magnification. The SEM micrographs show the uniform dispersion of MWCNTs within the PPR matrix and the inset images confirm the opening of CNT bundles and formation of CNT networks within the polymer matrix[28]. The uniform dispersion of MWCNTs and the formation of conductive networks indicate that the shear-induced melt-phase mixing in the extruder is an efficient approach for the development of nano-engineered composites. The uniform dispersion of fillers within the polymer is an important criterion for the development of self-sensing material as agglomerations may lead to inconsistent sensitivity. Further, as the MWCNTs impart reinforcing effect and are electrically conductive, it is expected that the composites display desirable mechanical properties and appreciable piezoresistive response.

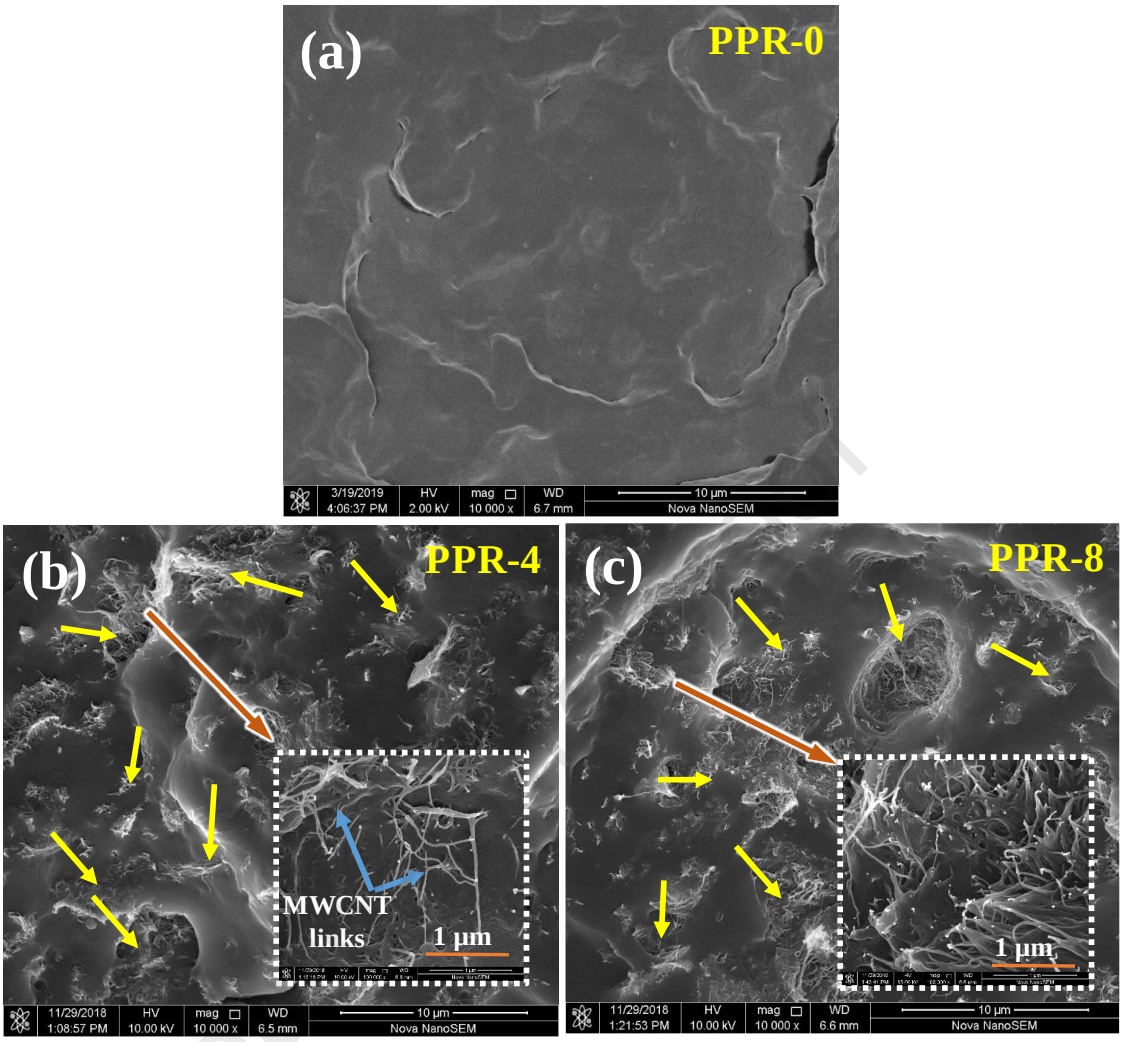

Fig.2 SEM micrographs of PPR/MWCNT composites with varying MWCNT content while inset images show SEM micrographs of same composition at higher magnification (100000X): a) neat PPR, b) PPR with 4wt.% MWCNT loading and c) PPR with 8wt.% MWCNT loading. Arrows indicate the MWCNT in PPR matrix.

3.2 Electrical conductivity of PPR/MWCNT composites

Electrical conductivity of PPR/MWCNT composites as a function of MWCNT wt.% has been measured and reported in our previous works [30, 31]. The conductivity measurements show that the electrical conductivity of PPR improves significantly with the addition of MWCNTs (2-8

wt.%), with a sharp increase in conductivity at 2 wt.% MWCNTs loading (from 10^{-11} to 10^{-7}S/cm). The sharp increase in the electrical conductivity of the composites indicates the formation of electrically conductive network within the insulating polymer. The formation of the first conducting network within the matrix is referred to as electrical percolation threshold, which can be calculated by calibrating the measured data using power-law model [32]. The percolation value for the PPR/MWCNT composites was observed to be ~1.40 wt.% [33].

3.3 Mechanical performance of PPR/MWCNT composites

It is well known that MWCNTs form clusters in the matrix due to strong van der Waals forces at higher CNT loading. As a result, the exceptional properties of CNTs cannot be effectively utilized. The deagglomeration and opening of MWCNT clusters facilitates the uniform dispersion of CNTs and creates viable interfaces between CNTs and the matrix. This is essential for the development of mechanically efficient multifunctional composites. Therefore, we investigated the mechanical properties of the composites to evaluate the reinforcing and stiffening effect of CNTs.

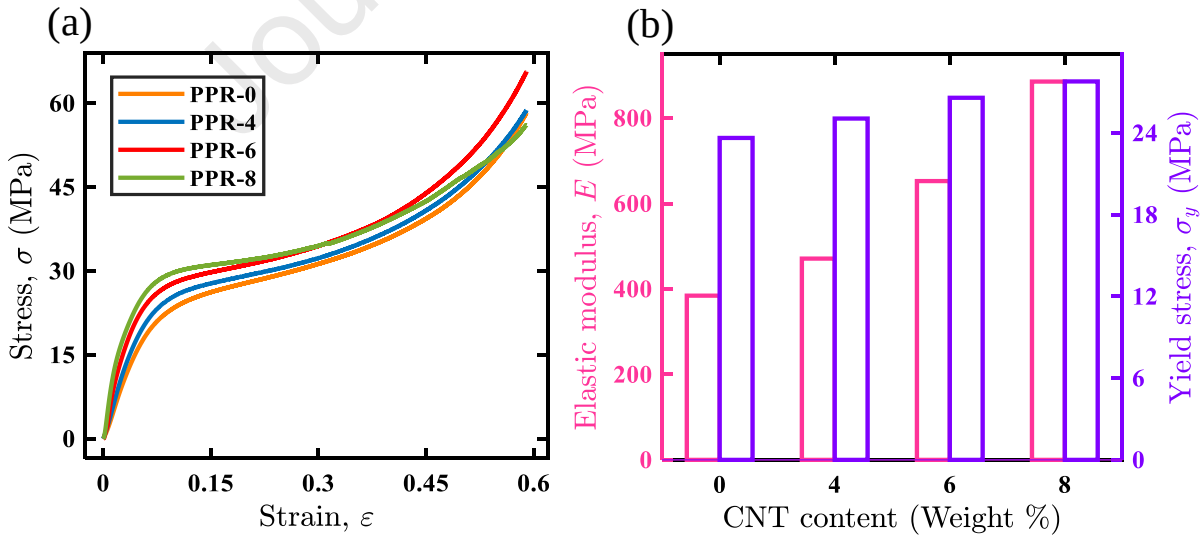

Fig.3. a) Representative compressive stress-strain response of 3D printed PPR/MWCNT bulk composites and b) elastic modulus and yield stress for different MWCNT loadings of composites.

The compressive mechanical performance of PPR/MWCNT composites is shown in Fig.3, where representative stress-strain responses of the neat PPR and PPR/MWCNT composite samples are shown. Fig.3a and Fig.3b show the compressive strength and modulus of the composites with varying MWCNT content. It can be seen (Fig.3b) that the addition of MWCNTs to PPR improves the compressive strength by 25%, i.e., from 24 MPa (for PPR-0) to 30 MPa (for PPR-8). The improved strength could be due to the efficient stress transfer to the CNTs from the matrix and the homogeneous dispersion of MWCNTs in the matrix. PPR-MWCNT interfaces act as load-bearing interfaces and the load is efficiently transferred from the matrix to the MWCNTs through such interfaces. In addition, inherent stiffness of MWCNTs and the ability of MWCNTs to enhance the melt crystallization of the PPR matrix, contribute to stiffening and strengthening [34]. Indeed, it is also observed that the elastic modulus of PPR (Fig. 3b) increased by ~25% and ~125% with the addition of 4 and 8 wt% MWCNTs, respectively, confirming that MWCNTs impart stiffness to the polymer matrix.

3.4. Piezoresistive characteristics of PPR/MWCNT composites

3.4.1. Effect of MWCNT loading

The piezoresistive strain sensitivity of a composite is defined in terms of the gauge factor (k), which can be determined by the slope of the normalized change in resistance vs. strain curve and can be expressed as follows.

$$k = \frac{d}{d\varepsilon}\left[\frac{\Delta R}{R_0}\right] = \frac{1}{R_0}\left[\frac{dR}{d\varepsilon}\right] \quad (1)$$

Where R_0 is the initial resistance of the composites, ΔR is the change in resistance due to change in imposed strain $'d\varepsilon'$.

Fig.4 shows the piezoresistive performance of PPR/MWCNT bulk composites under monotonic compression for varying amount of MWCNT. The graph (Fig.4) clearly shows that the composites with 4, 6 and 8 wt% MWCNT have k (sensitivity) values of 27.8, 20.7 and 17.1, respectively. Note that the gauge factor decreases with increasing MWCNT loading. When the strain approaches a critical value during mechanical compression loading, the CNT network is disturbed and the distance between MWCNTs decreases, leading to the formation of new conducting paths[35]. At this stage, the electrical conductivity or resistance change of the composites is determined by the contact junction resistance between the CNTs rather than electron tunnelling and hopping mechanisms (see, Fig. 5a & 5b). The occurrence of resistance changes at this time is due to a change in the morphology of the MWCNT network. The morphological changes during the compression test are also confirmed by Raman spectroscopy. From Fig. 5c and 5d, it can be seen that the I_D /I_G ratio is higher in the compressed samples (Fig. 5d) indicating more disordered structure (Fig. S1).

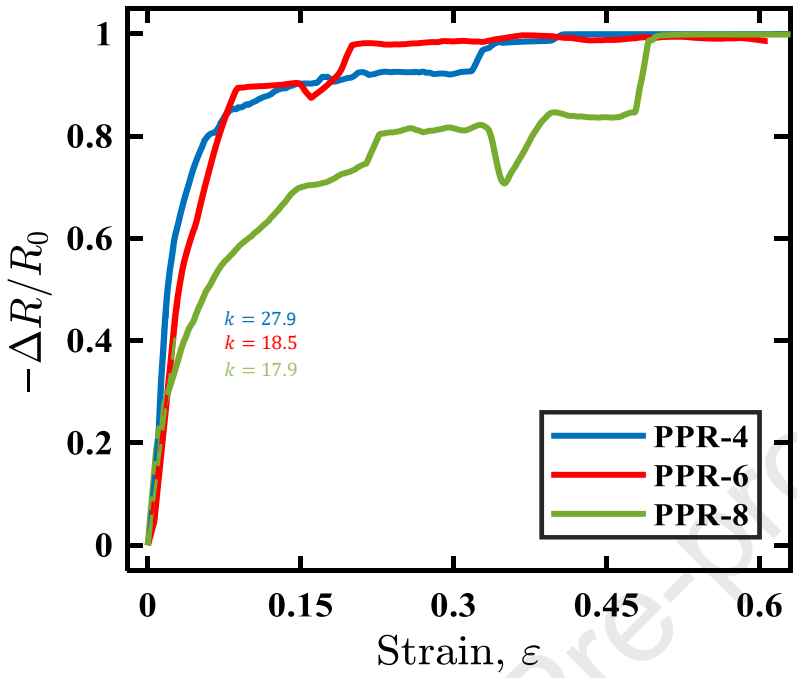

Fig.4 Evolution of normalized change in resistance during monotonic compressive loading of PPR/MWCNT composites with different CNT loadings.

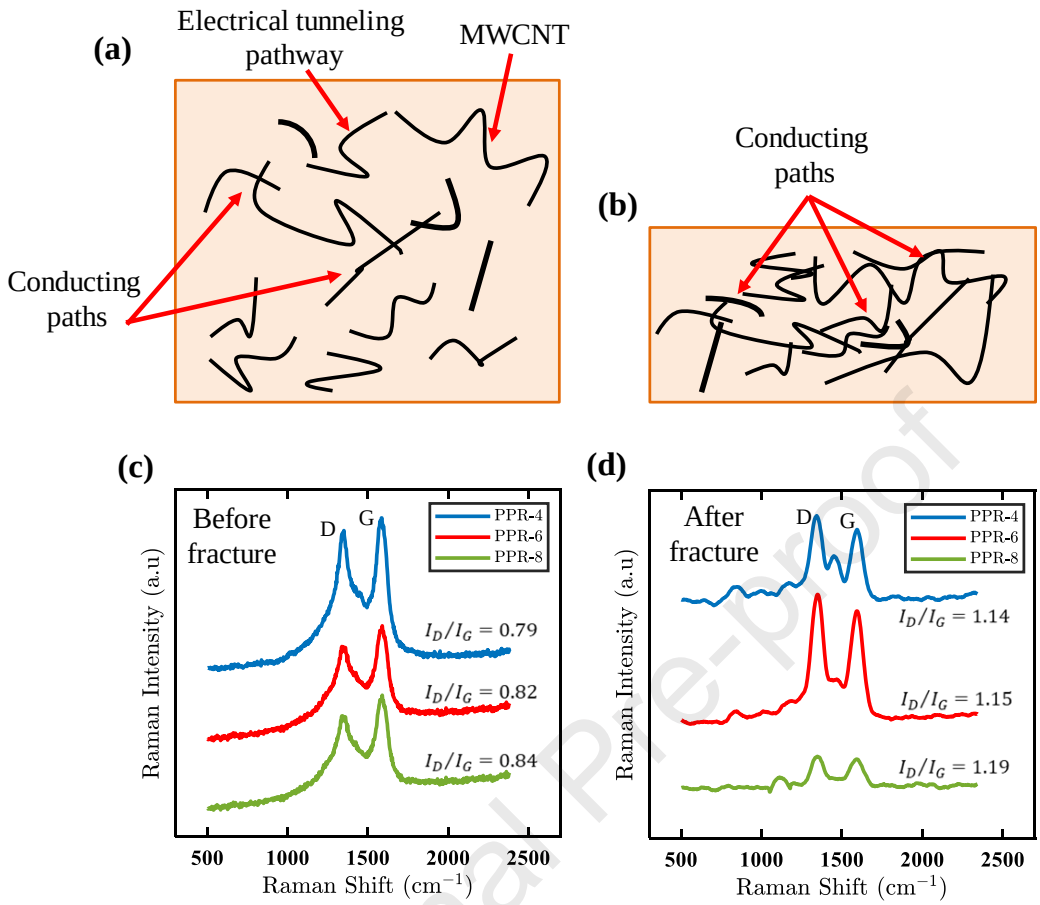

Fig.5a and 5b show the schematic of morphology of MWCNT network before and after the application of compressive load respectively while Fig.5c and 5d indicate corresponding Raman spectra**.**

3.4.2. Effect of strain-rate

The piezoresistive performance of polymer composites is based on the change in resistance due to the change in morphology of the conductive network and is expected to change with loading speed. Therefore, here we investigate the compressive piezoresistive behaviour of polymer composites by varying the strain rate. The gauge factors of the composites under compression with strain rates of 5, 25, and 50 mm/min were 27.9, 17.1, and 18.0, respectively, for the sample with 4 wt.% MWCNT loading (PPR-4). Likewise, the gauge factors of the composites loaded with 6 and 8

wt.% MWCNT also show similar trends and the results are summarized in Table 1. From Fig. 6, it can be seen that the gauge factor (sensitivity) generally decreases with increasing strain rate, which could be due to the faster reduction in the average separation distance between MWCNTs and the shorter response time at higher strain rate. Since the piezoresistive performance of PPR/MWCNT composites is affected by strain rate, it can be used as a guideline for developing self-sensing materials for high strain rate applications.

Table.1 Summary of gauge factors of different PPR composites under compression for different strain rates

Sample designations	Gauge factor (k) at different strain rates		
	k at 5 mm/min	k at 25 mm/min	k at 50 mm/min
PPR-4	27.9	17.1	18.0
PPR-6	18.5	16.8	14.9
PPR-8	17.9	15.7	14.3

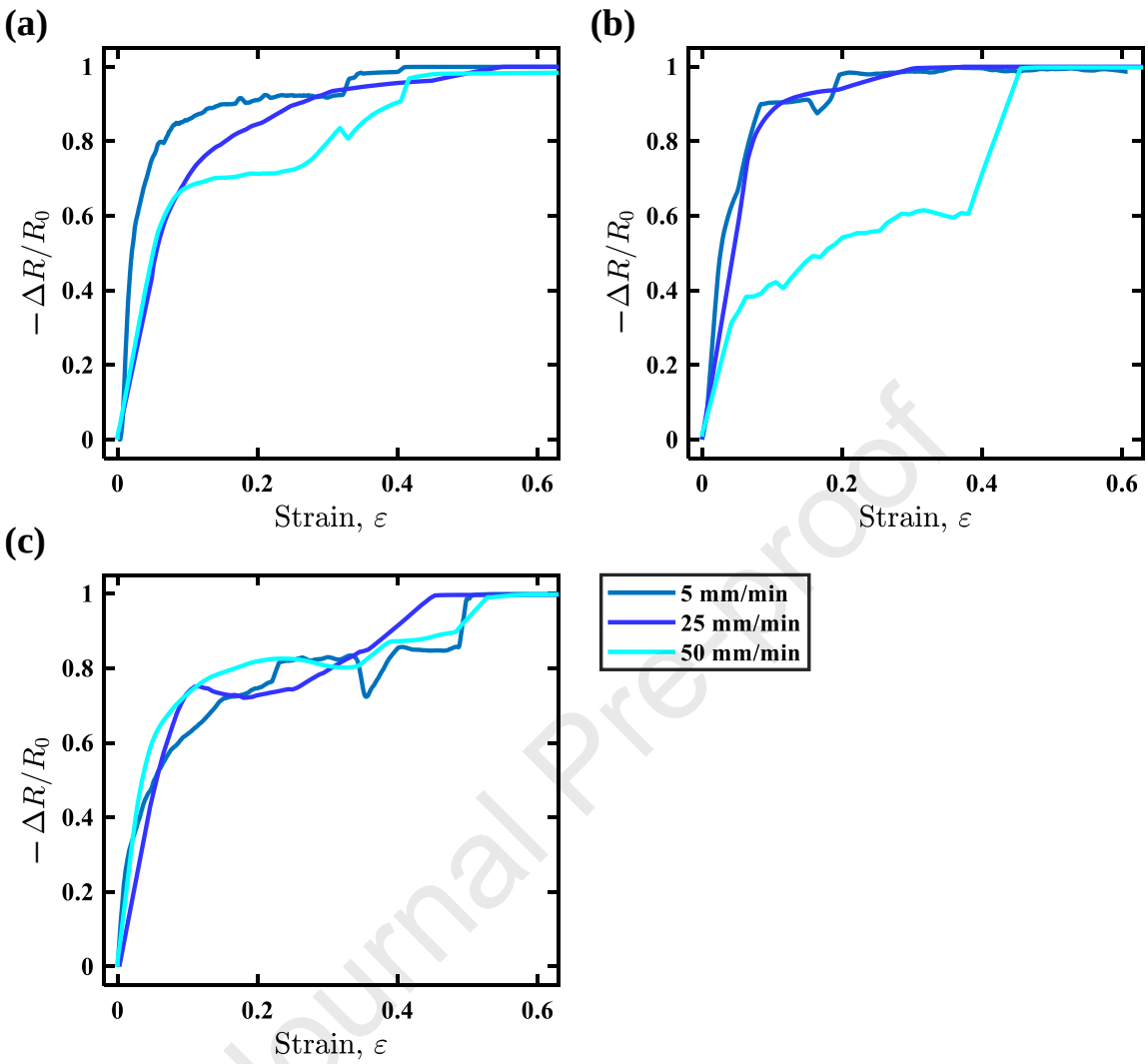

Fig.6. Effect of strain rate on piezoresistive response of PPR/MWCNT composites for different MWCNT loadings.

3.4.3. Piezoresistive response of nanocomposite under repeated quasi-static cyclic compression

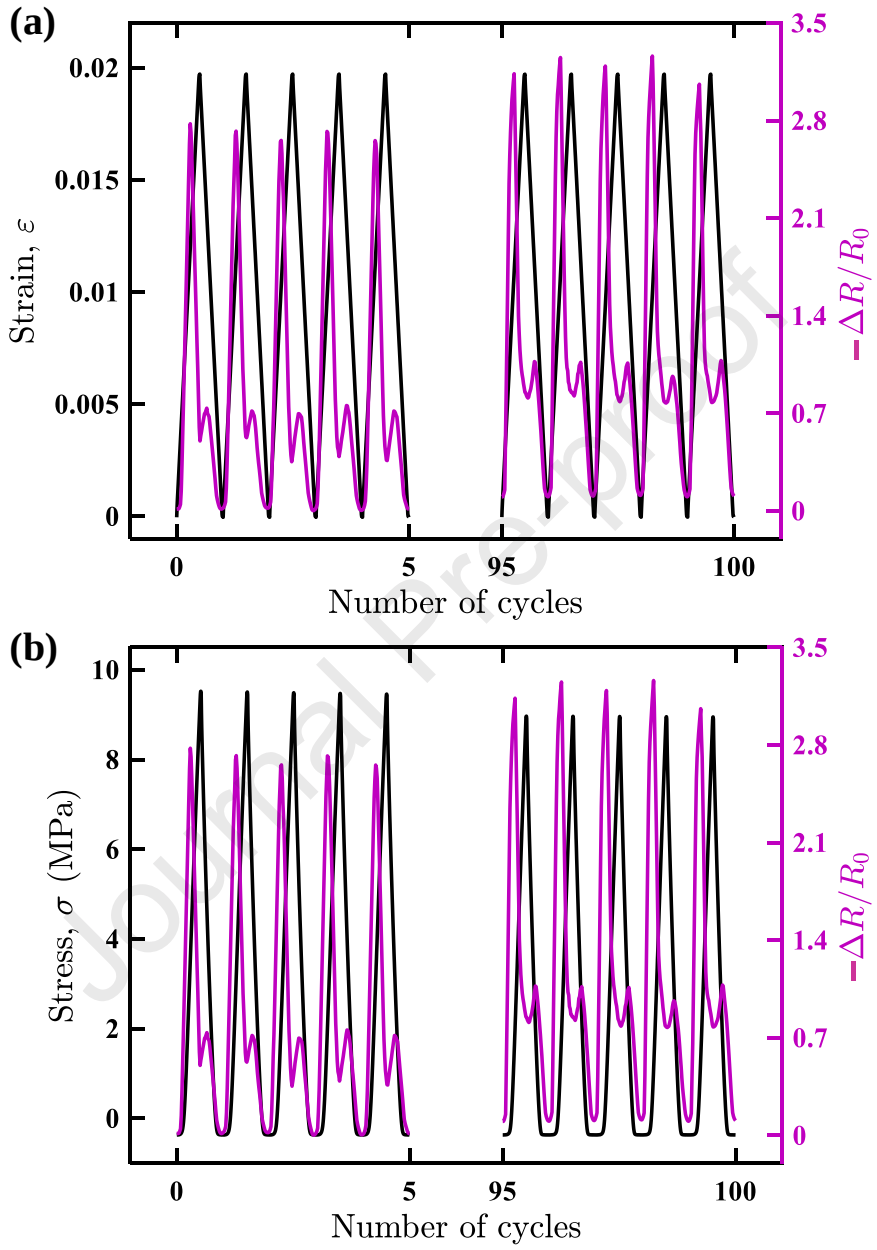

Fig.7. Piezoresistive response of PPR/MWCNT composites comprising 4 wt.% MWCNT loading, under cyclic compressive loading up to 100 cycles with a 2% strain amplitude: (a) evolution of normalized resistance change with applied strain as a function of number of cycles and (b) evolution of normalized resistance change and stress as a function of number of cycles.

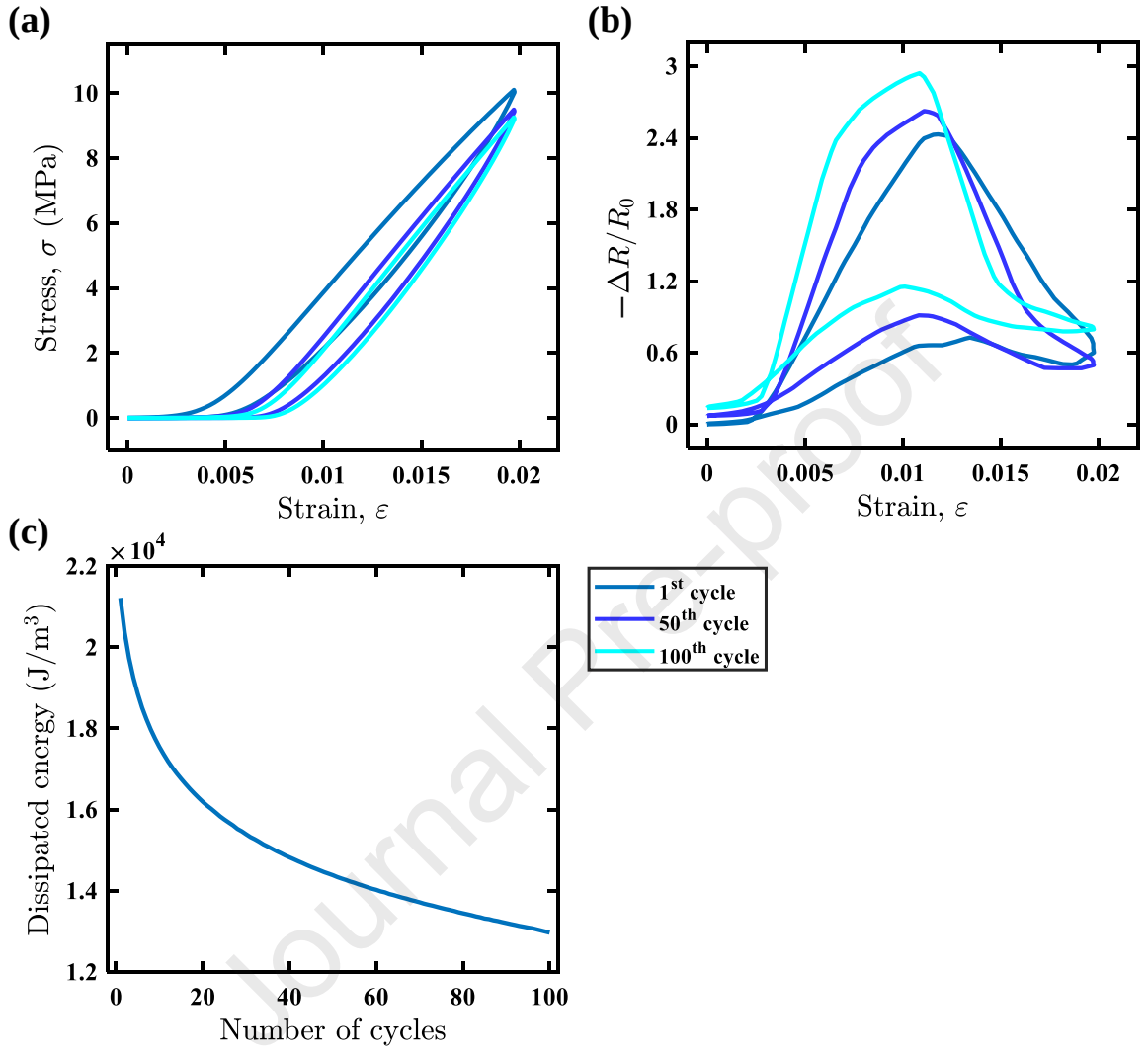

Fig.8 Piezoresistive performance of PPR/MWCNT composites comprising 4 wt.% MWCNT loading, under cyclic compressive loading up to 100 cycles with a of 2% strain amplitude: (a) hysteresis loop for 1st, 50th and 100thcycles, (b) -ΔR/R0-ε curve for 1st, 50th and 100th cycles and (c) dissipated energy vs. number of cycles.

PPR /MWCNT composite specimens containing 4 wt% MWCNT are tested under repeated cyclic compression loading up to 100 cycles with a strain amplitude of 2% (corresponding to the linear elastic regime) at a strain rate of 5 mm/min, as this composite showed good sensitivity under

monotonic compression loading (see Fig.4). Repeated cyclic loading with constant strain amplitude helps to evaluate the hysteresis performance of the composites. From Fig.7a and7b, it can be seen that the stress increases linearly to a maximum in response to the applied strain and returns to zero upon unloading, closing the hysteresis loop (Fig.8a). Interestingly, the normalized change in resistance during loading follows a similar trend. However, during unloading, the normalized resistance change shows a shoulder peak, unlike the stress-strain response. This response is attributed to the restructuring of the MWCNT networks due to the viscous nature of the polymer. During compression, the polymer chains are stretched by the load, reaching an entropically unstable state. As a result, the MWCNTs begin to move in the direction of mechanical deformation. The average spacing between nanotubes decreases, which leads to microstructural changes and thus alters the electrical resistance. When the cyclic strain persists, the PPR chains gradually return to their original position and reach an entropically stable state [25].

It is also observed that the peak stress decreases as the number of cycles increases (Fig. 8a & 8b). This cyclic softening behavior indicates the phenomenon of polymer chain relaxation. The decrease in the maximum stress with the number of cycles supports this observation. Although the peak stress decreases slightly between the 1st and 50th cycles, the peak stress is almost the same during the 50th and 100th cycles, confirming that the mechanical performance of the composites is stable up to 100 loading/unloading cycles at a strain amplitude of 2%. The dissipated energy as a function of the number of cycles (Fig.8c) also confirms the change of energy during cyclic loading.

3.4.4. Piezoresistive response of nanocomposite under quasi-static cyclic compression with increasing strain amplitude

The performance of the PPR /MWCNT composites samples (containing 4 wt% MWCNT) under incremental cyclic compression loading was evaluated. Fig. 9a & 9b show the $-\Delta R/R_0$ profile over 7 compression cycles with increasing strain amplitude, while Fig. 9c shows the corresponding stress-strain behaviour. As the strain amplitude increases and decreases, the $-\Delta R/R_0$ values also increase and decrease accordingly (see Fig.9a & 9b). The decrease in relative resistance change is due to the decrease in MWCNT-to-MWCNT distance due to incremental compressive loading. The signature of the shoulder peak in the sample at higher cycles could be due to rearrangements of the MWCNT network and accumulation of a residual strain with increasing number of cycles.

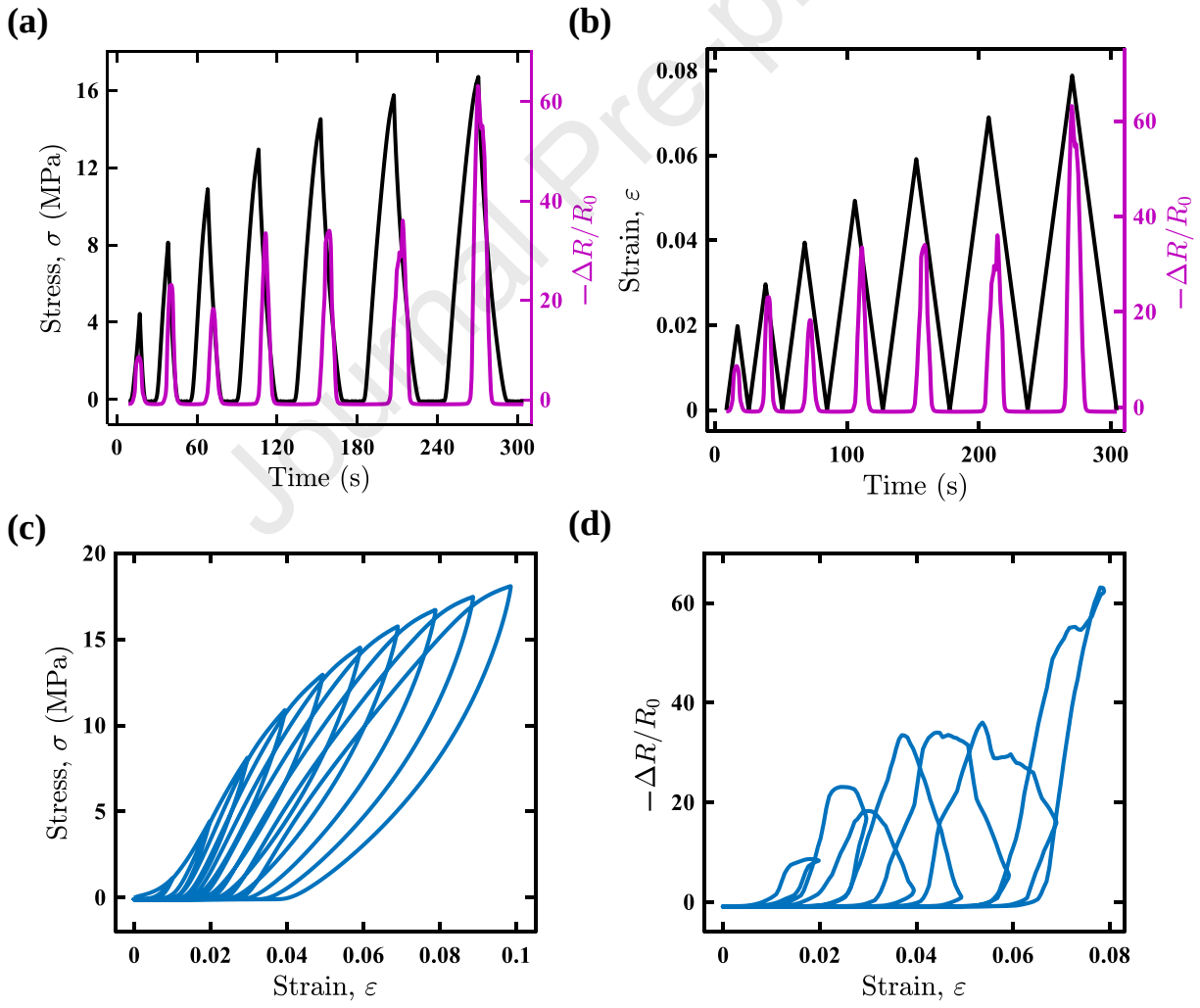

Fig.9 Cyclic loading with increasing strain amplitude: (a) and (b) variation of stress and strain and normalized resistance change (-ΔR/R₀) with time for PPR-4 respectively, (c) stress vs. strain response of PPR-4 samples and (d) normalized resistance change (-ΔR/R₀) vs. strain response of PPR-4 samples.

3.5. Piezoresistive performance of PPR/MWCNT plate-lattices under quasi-static compression

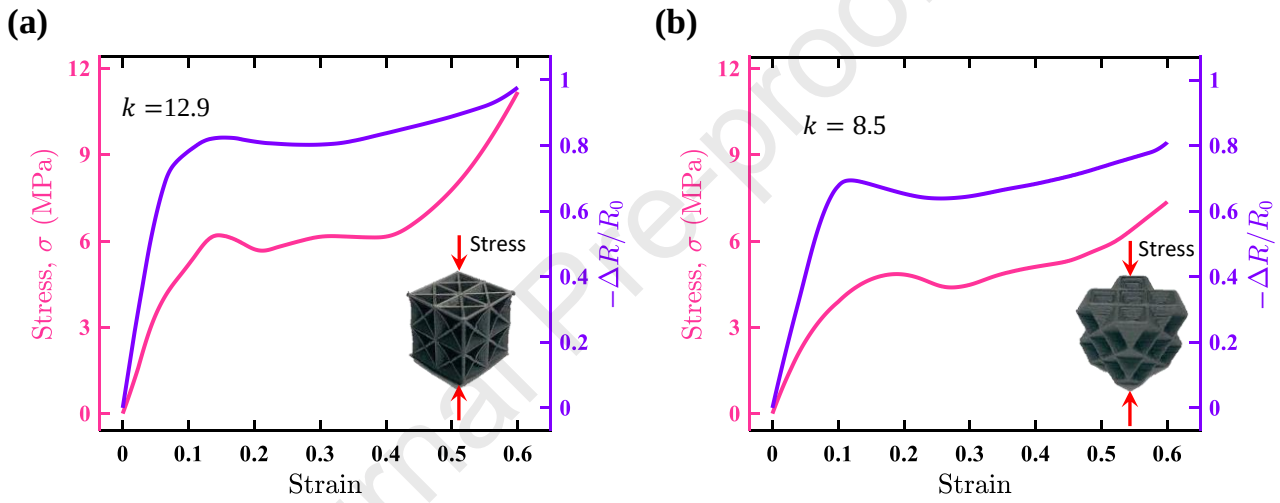

Fig.10 Piezoresistive response of PRR/MWCNT cellular composite structures comprising 4 wt.% MWCNT loading: (a) BCC plate-lattice and (b) FCC plate-lattice

Cellular structures with two different closed-cell architectures, namely BCC plate-lattice and FCC plate-lattice, were additively manufactured using PPR-4 (with 4 wt.% MWCNT loading) and the effect of the unit cell topology on mechanical and self-sensing performance of cellular architectures is evaluated. The out-of-plane engineering compressive stress-strain behaviour of the cellular structures obtained from quasi-static experiments are plotted in Fig.10. The modulus of the BCC and FCC structures was found to be 70 MPa and 56 MPa, respectively. Similarly, the gauge factor of the BCC and the FCC lattices was observed to be ~12.9 and ~8.5 respectively. The

higher modulus and gauge factor of BCC plate-lattice could be attributed to their greater extent of stretch-dominated deformation behaviour, while FCC plate-lattices exhibit more bend-dominated behaviour. Bend-dominated cellular structures are subjected to tensile stresses (or strains) and compressive stresses (or strains) at different locations in the plates. In tensile stress regions, the conducting paths reduce with load due to mechanisms such as the change in contact resistance between the CNTs and tunneling. Unlike FCC lattices, BCC structures are subject to stretching-dominant deformations. For this reason, BCC structures are expected to have a lower effect of tensile stresses (or strains) and thus have a higher sensitivity. This suggests the possibility of developing AM-enabled nano-engineered cellular structures with tunable mechanical and self-sensing properties suitable for a variety of applications. [36].

3.6. Piezoresistive performance comparison with extant works

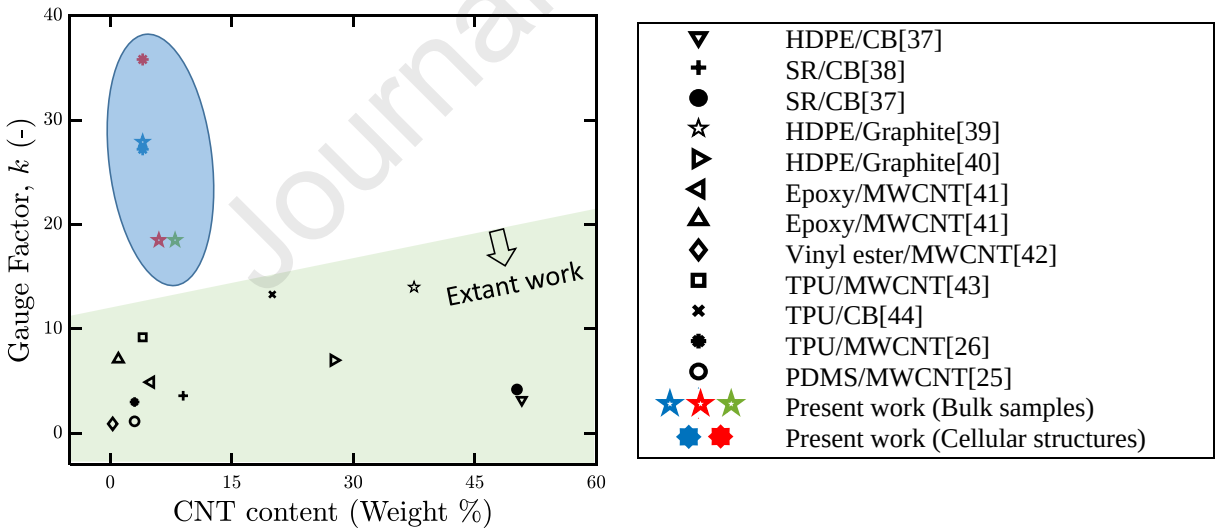

Fig.11 Comparison of the gauge factors obtained from present work with those of extant works.

In some recent studies [25, 26, 37-44], researchers have developed piezoresistive self-sensing composites using a variety of approaches. Fig. 11 compares the gauge factors of 3D-

printed bulk and cellular structures of PPR /MWCNT composites with those reported in the extant works. The results show that our AM-enabled structures exhibit excellent piezoresistive sensitivity compared to those of extant works. Our results show a superior gauge factor for the BCC cellular structure with 4 wt% MWCNT.

Conclusions

In this study, piezoresistive and mechanical behavior of additive manufacturing-enabled bulk and cellular PPR/MWCNT composites under monotonic and quasi-static cyclic compressive loading is presented. The composite filaments were fabricated by a shear-induced melt mixing process that facilitates a uniform dispersion of MWCNTs and the formation of conductive networks in the PPR matrix. MWCNT-based polymer composites showed excellent conductivity (up to ~10^{-1} S/cm) and good mechanical performance (compressive strength up to 30 MPa) along with remarkable piezoresistive sensing performance (with a sensitivity of 27.9 for bulk samples and excellent reversibility over 100 cycles). The cellular structures displayed tunable piezoresistive (gauge factor) and mechanical (modulus) performance, i.e., ~12.9 and 70 MPa for BCC plate-lattice and ~8.5 and 56 MPa for FCC plate-lattice, respectively. This study presents an industrially viable, low-cost process that can be used to develop highly sensitive, lightweight bulk and cellular composites with tunable sensitivity and mechanical response. The research findings from the study can be applied to industrial robots, lightweight smart structures and electronics for rehabilitation or failure prevention.

Acknowledgement

Authors gratefully acknowledge financial support from the Abu Dhabi National Oil Company (ADNOC), United Arab Emirates under Award No: EX2016-000010.

Reference

[1] W. Bauhofer, J.Z. Kovacs, A review and analysis of electrical percolation in carbon nanotube polymer composites, Composites Science and Technology 69(10) (2009) 1486-1498.
[2] A. Mora, P. Verma, S. Kumar, Electrical conductivity of CNT/polymer composites: 3D printing, measurements and modeling, Composites Part B: Engineering 183 (2020) 107600.
[3] I. Kang, M.J. Schulz, J.H. Kim, V. Shanov, D. Shi, A carbon nanotube strain sensor for structural health monitoring, Smart materials and structures 15(3) (2006) 737.
[4] S. Kumar, T.K. Gupta, K. Varadarajan, Strong, stretchable and ultrasensitive MWCNT/TPU nanocomposites for piezoresistive strain sensing, Composites Part B: Engineering 177 (2019) 107285.
[5] M.F. Arif, S. Kumar, T.K. Gupta, K.M. Varadarajan, Strong linear-piezoresistive-response of carbon nanostructures reinforced hyperelastic polymer nanocomposites, Composites Part A: Applied Science and Manufacturing 113 (2018) 141-149.
[6] S.P. Patole, S.K. Reddy, A. Schiffer, K. Askar, B.G. Prusty, S. Kumar, Piezoresistive and mechanical characteristics of graphene foam nanocomposites, ACS Applied Nano Materials 2(3) (2019) 1402-1411.
[7] G. Choi, J. Lee, J. Cha, Y.-J. Kim, Y.-S. Choi, M. Schulz, C. Moon, K. Lim, S. Kim, I. Kang, A spray-on carbon nanotube artificial neuron strain sensor for composite structural health monitoring, Sensors 16(8) (2016) 1171.
[8] M. Nadgorny, A. Ameli, Functional polymers and nanocomposites for 3D printing of smart structures and devices, ACS applied materials & interfaces 10(21) (2018) 17489-17507.
[9] M. Hofmann, 3D printing gets a boost and opportunities with polymer materials, ACS Publications, 2014.
[10] X. Wang, M. Jiang, Z. Zhou, J. Gou, D. Hui, 3D printing of polymer matrix composites: A review and prospective, Composites Part B: Engineering 110 (2017) 442-458.
[11] B. Khoshnevis, Automated construction by contour crafting—related robotics and information technologies, Automation in Construction 13(1) (2004) 5-19.
[12] K. Gnanasekaran, T. Heijmans, S. Van Bennekom, H. Woldhuis, S. Wijnia, G. de With, H. Friedrich, 3D printing of CNT-and graphene-based conductive polymer nanocomposites by fused deposition modeling, Applied materials today 9 (2017) 21-28.
[13] J.J. Andrew, H. Alhashmi, A. Schiffer, S. Kumar, V.S. Deshpande, Energy absorption and self-sensing performance of 3D printed CF/PEEK cellular composites, Materials & Design 208 (2021) 109863.
[14] R.D. Farahani, M. Dubé, D. Therriault, Three-dimensional printing of multifunctional nanocomposites: manufacturing techniques and applications, Advanced materials 28(28) (2016) 5794-5821.
[15] K. Gnanasekaran, T. Heijmans, S. van Bennekom, H. Woldhuis, S. Wijnia, G. de With, H. Friedrich, 3D printing of CNT- and graphene-based conductive polymer nanocomposites by fused deposition modeling, Applied Materials Today 9 (2017) 21-28.
[16] O.A. Mohamed, S.H. Masood, J.L. Bhowmik, Parametric Analysis of the Build Cost for FDM Additive Processed Parts Using Response Surface Methodology, Reference Module in Materials Science and Materials Engineering, Elsevier2016.
[17] S. Berretta, R. Davies, Y.T. Shyng, Y. Wang, O. Ghita, Fused Deposition Modelling of high temperature polymers: Exploring CNT PEEK composites, Polymer Testing 63 (2017) 251-262.
[18] G.M. Rizvi, C.T. Bellehumeur, P. Gu, Q. Sun, Effect of processing conditions on the bonding quality of FDM polymer filaments, Rapid Prototyping Journal 14(2) (2008) 72-80.
[19] R. Melnikova, A. Ehrmann, K. Finsterbusch, 3D printing of textile-based structures by Fused Deposition Modelling (FDM) with different polymer materials, IOP conference series: materials science and engineering, IOP publishing, 2014, p. 012018.

[20] B. Tymrak, M. Kreiger, J.M. Pearce, Mechanical properties of components fabricated with open-source 3-D printers under realistic environmental conditions, Materials & Design 58 (2014) 242-246.
[21] P. Tran, T.D. Ngo, A. Ghazlan, D. Hui, Bimaterial 3D printing and numerical analysis of bio-inspired composite structures under in-plane and transverse loadings, Composites Part B: Engineering 108 (2017) 210-223.
[22] B. Caulfield, P. McHugh, S. Lohfeld, Dependence of mechanical properties of polyamide components on build parameters in the SLS process, Journal of Materials Processing Technology 182(1-3) (2007) 477-488.
[23] C.R. Garcia, J. Correa, D. Espalin, J.H. Barton, R.C. Rumpf, R. Wicker, V. Gonzalez, 3D printing of anisotropic metamaterials, Progress In Electromagnetics Research 34 (2012) 75-82.
[24] M.R. Dusseiller, D. Schlaepfer, M. Koch, R. Kroschewski, M. Textor, An inverted microcontact printing method on topographically structured polystyrene chips for arrayed micro-3-D culturing of single cells, Biomaterials 26(29) (2005) 5917-5925.
[25] M. Abshirini, M. Charara, P. Marashizadeh, M.C. Saha, M.C. Altan, Y. Liu, Functional nanocomposites for 3D printing of stretchable and wearable sensors, Applied Nanoscience (2019) 1-13.
[26] J. Christ, N. Aliheidari, P. Pötschke, A. Ameli, Bidirectional and Stretchable Piezoresistive Sensors Enabled by Multimaterial 3D Printing of Carbon Nanotube/Thermoplastic Polyurethane Nanocomposites, Polymers 11(1) (2019) 11.
[27] J. Ubaid, J. Schneider, V.S. Deshpande, B.L. Wardle, S. Kumar, Multifunctionality of Nanoengineered Self-Sensing Lattices Enabled by Additive Manufacturing, Adv. Eng. Mater. 24(7) (2022) 2200194.
[28] P. Verma, P. Saini, R.S. Malik, V. Choudhary, Excellent electromagnetic interference shielding and mechanical properties of high loading carbon-nanotubes/polymer composites designed using melt recirculation equipped twin-screw extruder, Carbon 89 (2015) 308-317.
[29] M.F. Arif, H. Alhashmi, K.M. Varadarajan, J.H. Koo, A.J. Hart, S. Kumar, Multifunctional performance of carbon nanotubes and graphene nanoplatelets reinforced PEEK composites enabled via FFF additive manufacturing, Composites Part B: Engineering 184 (2020) 107625.
[30] P. Verma, J. Ubaid, K.M. Varadarajan, B.L. Wardle, S. Kumar, Synthesis and Characterization of Carbon Nanotube-Doped Thermoplastic Nanocomposites for the Additive Manufacturing of Self-Sensing Piezoresistive Materials, ACS Applied Materials & Interfaces 14(6) (2022) 8361-8372.
[31] P. Verma, T. Bansala, S.S. Chauhan, D. Kumar, S. Deveci, S. Kumar, Electromagnetic interference shielding performance of carbon nanostructure reinforced, 3D printed polymer composites, Journal of Materials Science 56(20) (2021) 11769-11788.
[32] P. Verma, P. Saini, V. Choudhary, Designing of carbon nanotube/polymer composites using melt recirculation approach: Effect of aspect ratio on mechanical, electrical and EMI shielding response, Materials & Design 88 (2015) 269-277.
[33] T. Bansala, M. Joshi, S. Mukhopadhyay, R.-A. Doong, M. Chaudhary, Electrical and Dielectric Properties of Exfoliated Thermally Reduced Graphene Based Polyurethane Nanocomposites, Journal of Nanoscience and Nanotechnology 17(12) (2017) 8782-8790.
[34] P. Verma, V. Choudhary, Polypropylene random copolymer/MWCNT nanocomposites: Isothermal crystallization kinetics, structural, and morphological interpretations, Journal of Applied Polymer Science 132(13) (2015).
[35] D. Cho, J. Park, J. Kim, T. Kim, J. Kim, I. Park, S. Jeon, Three-Dimensional Continuous Conductive Nanostructure for Highly Sensitive and Stretchable Strain Sensor, ACS Applied Materials & Interfaces 9(20) (2017) 17369-17378.
[36] S. Kumar, J. Parakkal, A. Rajkumar, A. Schiffer, V. Deshpande, Tunable Energy Absorption Characteristics of Architected Honeycombs Enabled via Additive Manufacturing, ACS Applied Materials & Interfaces (2019).

[37] P. Wang, T. Ding, Conductivity and piezoresistivity of conductive carbon black filled polymer composite, Journal of applied polymer science 116(4) (2010) 2035-2039.
[38] W.E. Mahmoud, A. El-Lawindy, M. El Eraki, H. Hassan, Butadiene acrylonitrile rubber loaded fast extrusion furnace black as a compressive strain and pressure sensors, Sensors and Actuators A: Physical 136(1) (2007) 229-233.
[39] Q. Zheng, Y. Song, X.-S. Yi, Piezoresistive properties of HDPE/graphite composites, Journal of materials science letters 18(1) (1999) 35-37.
[40] J. Lu, X. Chen, W. Lu, G. Chen, The piezoresistive behaviors of polyethylene/foliated graphite nanocomposites, European Polymer Journal 42(5) (2006) 1015-1021.
[41] G. Yin, N. Hu, Y. Karube, Y. Liu, Y. Li, H. Fukunaga, A carbon nanotube/polymer strain sensor with linear and anti-symmetric piezoresistivity, Journal of composite materials 45(12) (2011) 1315-1323.
[42] J. Ku-Herrera, F. Avilés, G. Seidel, Self-sensing of elastic strain, matrix yielding and plasticity in multiwall carbon nanotube/vinyl ester composites, Smart Materials and Structures 22(8) (2013) 085003.
[43] J.F. Christ, N. Aliheidari, A. Ameli, P. Pötschke, 3D printed highly elastic strain sensors of multiwalled carbon nanotube/thermoplastic polyurethane nanocomposites, Materials & Design 131 (2017) 394-401.
[44] Z. Wang, X. Guan, H. Huang, H. Wang, W. Lin, Z. Peng, Full 3D Printing of Stretchable Piezoresistive Sensor with Hierarchical Porosity and Multimodulus Architecture, Advanced Functional Materials 29(11) (2019) 1807569.

Declaration of interests

☒ The authors declare that they have no known competing financial interests or personal relationships that could have appeared to influence the work reported in this paper.

☐The authors declare the following financial interests/personal relationships which may be considered as potential competing interests: